Journal of Minerals and Materials Characterization and Engineering, 2022, 10, 57-80
https://www.scirp.org/journal/jmmce
ISSN Online: 2327-4085
ISSN Print: 2327-4077

Recovery of Cassiterite and Topaz Minerals from an Old Metallurgical Dump, Eastern Desert of Egypt

Suzan Sami Ibrahim[1*], Khaled Ezzat Yassin[1], Tawfik Refaat Boulos[1], Ayman Aly Hagrass[2]

[1]Central Metallurgical Research and development Institute (CMRDI), Cairo, Egypt
[2]Tabbin Institute for Metallurgical Studies (TIMS), Cairo, Egypt
Email: *suzansibrahim@gmail.com, khaled_yassin@yahoo.com, trboulos83@gmail.com, aahagrass@gmail.com

How to cite this paper: Ibrahim, S.S., Yassin, K.E., Boulos, T.R. and Hagrass, A.A. (2022) Recovery of Cassiterite and Topaz Minerals from an Old Metallurgical Dump, Eastern Desert of Egypt. *Journal of Minerals and Materials Characterization and Engineering*, **10**, 57-80.
https://doi.org/10.4236/jmmce.2022.101005

Received: December 1, 2021
Accepted: January 26, 2022
Published: January 29, 2022

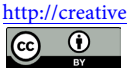

Abstract

Huge amounts of tailing dumps as a result of mines' blasting operations were impacting economic and environmental problems. Evaluation of one of these tailing dumps of the Eastern Desert of Egypt showed the presence of reasonable amount of cassiterite mineral reaching 0.199% SnO_2. The mineral cassiterite was found as finely disseminated particulates, reached to 5 microns, within varieties of quartz-feldspar-hornblende-biotite granitic formations. In the present study, the processing regime considered from the beginning the alignment between reaching cassiterite mineral liberation size, and its extreme brittleness character. Stirring ball milling technique was applied to produce −0.51 mm product with minimum fines as possible, which was left aside for a separate study. The ground product −0.51 + 0.074 mm was subjected to joint shaking table/dry high intensity magnetic separation techniques after splitting it into two fractions, −0.51 + 0.21 mm and −0.21 + 0.074 mm. Each fraction was separately subjected to "Wilfley" shaking table. At optimum conditions, a shaking table concentrate was obtained with 0.29% SnO_2 and an operational recovery reached 96.94% from a feeding contained 0.19% SnO_2. The heavies and the two middling products after shaking table were directed separately after dryness to dry high intensity magnetic separation using "Eriez" rare earth roll separator, meanwhile the light fractions were rejected. Mathematically designed experiments were applied to optimize the separation process. At optimum conditions, a final cassiterite concentrate was obtained with 11.25% SnO_2, and an operational recovery 94.08%. In addition, a topaz mineral concentrate was separated at splitter angle 65˚.

Keywords

Cassiterite, Shaking Table, Rare Earth Roll Magnetic Separator

1. Introduction

Cassiterite is considered to be the only economically significant tin mineral in the earth's crust. The mineral is hard and heavy, but also extremely brittle. Cassiterite has the chemical formula SnO_2 (78.8% Sn, and 21.2% O_2), density of 7.02 g/cm^3, and Mohs hardness 6 - 7. Cassiterite is of black, brown-black, yellowish brown, reddish brown coloration. It is nonmagnetic and conductive for electricity [1] [2] [3] [4].

Cassiterite mineral is almost enriched in the "tin granites", which contain approximately 15 - 50 g Sn/ton. It is found also as "mine tin" in domes of granite intrusions, in feldspar-topaz granites, and titano-magnetite deposits. Because it is very resistant to all weathering influences, it is a typical placer mineral. There are no specifications for commercial concentrates of cassiterite because it is always smelted directly, depending on the concentration, without further treatment [5] [6].

However, its high hardness property is accompanied by the unfortunate quality of extreme brittleness. This factor must be considered during the size reduction operations prior to concentration. Therefore, the general policy is that cassiterite grains should, where possible, be recovered at the earliest possible stage and at their largest size to avoid softness that is difficult to handle [7] [8].

It is obvious from the physical characteristics of cassiterite that its high relative specific gravity in relation to those of accompanied minerals constituents, in most cases, makes it an ideal mineral for the application of gravity-separation techniques. However, development of cassiterite beneficiation techniques has been carried out using flotation, electro and bio-flotation [9]-[23]. Sometimes, cassiterite was also could be separated using different magnetic separation techniques [24]-[33]. Microwave pre-treatment and hydrometallurgical methods were adapted also to recover cassiterite mineral and extract the tin metal [34]-[41].

However, all mines generate waste which are being stored at or near the mine site itself. Mine site rehabilitation can be expensive, and often the burden falls on the taxpayer rather than the mining company. This burden could be minimized if mining companies change their perception and start to view these disused materials not as waste, but as potential resources. Among these mines, are those locating in the Egyptian Eastern Desert that contains very large quantities of mine blasting remnants which are accumulated after different mining operations (**Figure 1**) [1]. Many scientific studies have succeeded to a large extent in developing research plans to concentrate many important minerals from these wastes such as gold, silver, copper, lead and zinc, and other important ores. However, very few studies have been devoted to recovering the mineral cassiterite. Therefore, this study aims to assess the extent to which a sample of these mining tails of cassiterite ores is capable of upgrading by simple physical techniques to obtain from them economically acceptable products for complementary industries.

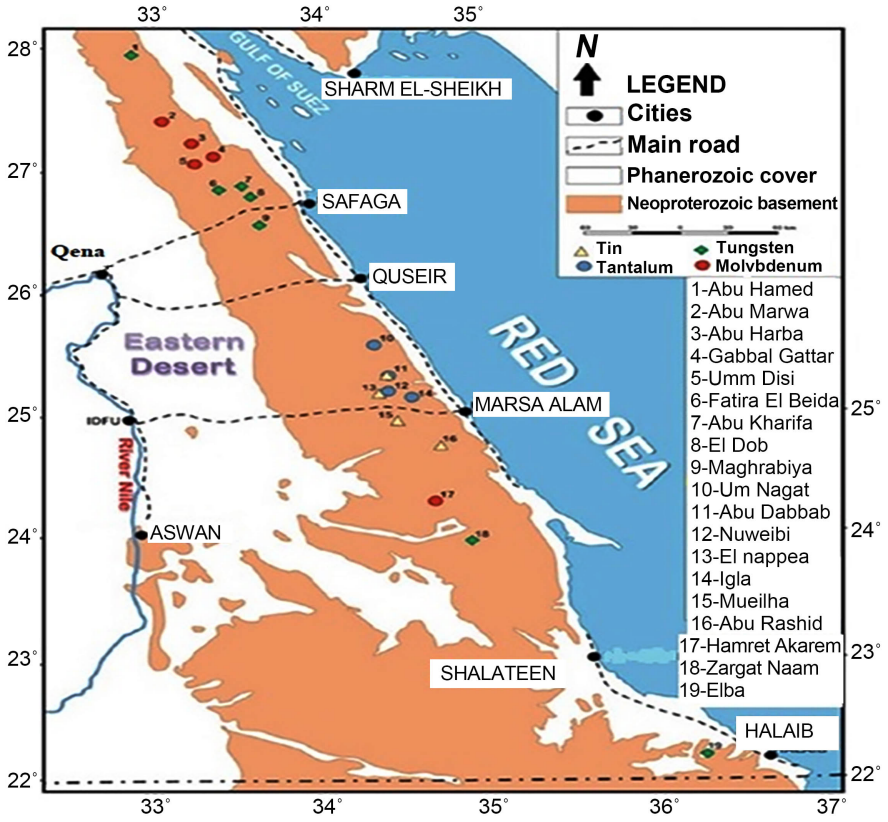

Figure 1. Occurrences of cassiterite deposits in the eastern desert of Egypt [42].

2. Methodology

A technological sample from the tailing dumps of the Eastern Desert of Egypt was supplied for evaluation and treatment. The sample was about −6 mm in size. It was subjected to elemental evaluation using XRF unit model PANalytical-Axios, and Perkin-Elmer Analyst 200 atomic absorption units. Phase analysis was applied using X-ray diffract-meter model "pw 1010" with CuKα radiation under target voltage 40 kV and current 30 mA in a scanning rate of 5˚ 2θ/min. Scanning electron microscope (SEM) type JEM-1230, JEOL equipped with energy dispersive X-ray (EDX) spectrometers was used to evaluate the final products.

A representative sample at the size fraction −6.0 + 2.28 mm from the original sample (14% by wt.) was divided into different cuts according to color. Polished sections of these samples were prepared for reflected light microscope investigation. Size reduction of the sample was conducted via stirring ball milling technique using wet batch laboratory mill Union Process "Attritor" model 1S, with working capacity 4.2 liters. The attrition time was conducted for 15 min as three steps, in closed circuit with 0.50 mm vibrating screen. The stirring speed was 1500 rpm, and the solid/water/balls ratio was 1/1/1 by wt. (each 800 g). The grinding zirconium ball diameter was 2 mm. The wet ground product was further screened on 0.074 mm sieve. Both the over and under screens products were collected, dried, and directed to evaluation. The under screen −0.074 mm fines

were kept aside for a separate study. The over screen product was further divided after dryness into −0.51 + 0.21 mm and -0.211 + 0.074 mm fractions for gravity and magnetic separation treatment.

The size fractions −0.51 + 0.211 mm and −0.211 + 0.074 mm were subjected separately to a "Wilfley" shaking table. Throughout the experiments, the samples were kept in suspension at 20% - 25% solids by weight with continuous mechanical stirring. However, the slurry was fed onto the inclined table surface at feeding rate of 1.30 kg/min. The wash water flow rate was kept at 20 l/min with table speed 300 rpm. Stroke length and deck inclination were optimized throughout the separation study. The middling and light products were further subjected to tabling separation at relatively lesser wash water flow rate, lesser tilt, and a shorter stroke length. An increase in the wash water flow rate showed separation improvement. As wash water flow rate increased, the transport of light minerals to the tailings fraction increased which in turn improved the separation. Improving in the heavy fraction was noticed at higher level of both deck tilt angle and feed flow rate [23] [35] [36] [37] [44].

At the end of shaking table process, various products were collected, dried, and directed to evaluation. Heavy and the two middling products were fed separately onto laboratory "Eriez" rare earth roll (RER) dry high intensity magnetic separator at permanent field strength of 21,000 gauss. Feeding rate was adjusted at 2 kg/ hr. Box-Behnken Design (BBD) [45] was constructed to optimize the separation process. The working variables were the separator splitter inclination angle and the roll belt speed. On the other hands, cassiterite recovery% was the sole response of the design (**Table 1**). The products after magnetic separation were directed to evaluation.

Software package, Design-Expert 6.0.5, Stat-Ease, Inc., Minneapolis, USA, was used for regression analysis of experimental data and to plot the response surface. Analysis of variance (ANOVA) was used to estimate the statistical parameters. The extent of fitting the experimental results to the polynomial model equation was expressed by the determination coefficient, R^2. F-test was used to estimate the significance of all terms in the polynomial equation within 95% confidence interval.

3. Results and Discussion

3.1. Sample Characterization

Results of XRF analysis showed that the sample contained 0.199% SnO_2. Major oxides were SiO_2, Al_2O_3, MgO, Fe_2O_3, and CaO, with 51.94%, 11.87%, 10.97%, 8.73%, and 5.68% contents, respectively (**Table 2**). They were related to different

Table 1. Levels of the two variable parameters.

Variable	Symbol	Unit	(−)	(0)	(+)
Splitter angle	A	degree	70.00	72.50	75.00
Belt speed	B	rpm	100	150	200

Table 2. XRF elemental analysis of original sample.

Oxide	Wt%	Oxide	Wt%
Na_2O	0.615	NiO	0.083
MgO	10.967	CuO	0.011
Al_2O_3	11.869	ZnO	0.008
SiO_2	51.939	As_2O_3	0.000
P_2O_3	o.292	Rb_2O	0.014
SO_3	0.031	SrO	0.014
K_2O	1.490	ZrO_2	0.021
CaO	5.683	Nb_2O_5	0.002
TiO_2	0.754	SnO_2	0.199
Cr_2O_3	0.175	PbO	0.007
MnO	0.402	Cl	0.004
Fe_2O_3	8.730		

minerals phases, e.g. albite, quartz, tremolite, clinochlore hornblende, biotite, and talc (Figure 2). According to XRD pattern, semi quantitative analysis, these phases represented about 27.30%, 22.8%, 12.30%, 21.90%, 11.70%, and 4.00%, respectively, of the original sample (Figure 2). The sample could be grouped according to density into light minerals and heavy minerals. The lights included albite, quartz, clinochlore, and talc with average density 2.65 g/cc. On the other side, heavy minerals included hornblende, tremolite, and biotite with average density 3.50 g/cc. Rare earth oxides e.g. ZrO_2, Rb_2O, SrO, and Nb_2O_5 assayed 0.021%, 0.014%, 0.014%, and 0.002% were identified (Table 1). Amounts of nickel, copper, and zinc oxides were also detected (Table 2). Size/chemical analyses of the original sample (as received) are shown in Table 3. It is clear that cassiterite showed concentration in SnO_2 reaching 0.39% - 0.25% in 0.59 - 0.074 mm fractions (Table 2). Fewer cassiterite concentrations assayed 0.17% to 0.11% SnO_2 were noted in coarser fractions 6.0 - 0.83 mm, and in the finer fraction −0.074 mm (Table 3).

The evaluation of the −6 + 2 mm fraction as major and minor components according to weight% was shown in Figure 3(A) and Figure 3(B), respectively. The major components represented about 58%, 18%, 9%, 5%, and 3%, by wt. of the fraction sample, respectively (Figure 3(A)). On the other hands, the minor components 6, 7, and 8 represented about 4% by wt. of the overall fraction sample −6.0 + 2.1 mm, where few particles of components 9 (mainly metallic particles), and component 10 (mainly mica) were found (Figure 3(B)). The semi-quantitative XRD analyses of these components were shown in Table 4.

On the other hands, Table 5 illustrates the size/chemical analyses of the ground product after the attritor. It was noted that low content of fines below 0.074 mm reaching about 15% by wt., were produced after the attritor milling process (Table 5). The constitution of these fines besides cassiterite may include the soft minerals e.g. talc and clinochlore.

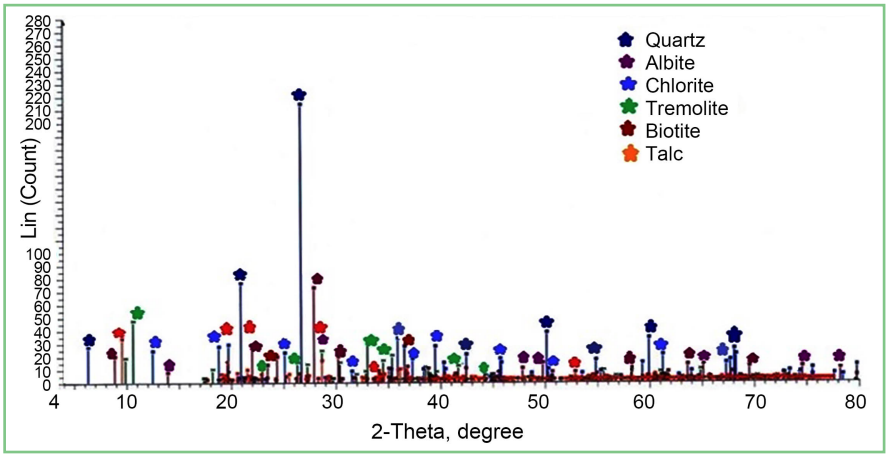

Figure 2. XRD Analysis of original sample.

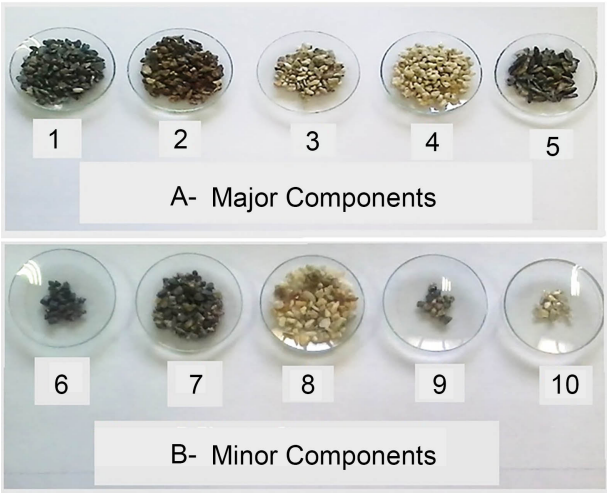

Figure 3. Major components of −6.0 + 2.23 mm original fraction.

Table 3. Size/chemical analysis of the original sample (as received).

Fraction, mm	Wt%	Cum.Wt%	SiO_2%	Al2O3%	Fe_2O_3%	SnO_2%
−6.0 + 1.168	14.60	14.60	47.66	5.25	7.66	0.17
−1.168 + 0.833	11.00	25.76	47.66	5.25	7.66	0.17
−0.83 + 0.598	10.10	36.66	45.52	5.65	7.39	0.38
−0.59 + 0.417	10.80	47.61	49.83	5.45	7.40	0.39
+0.295	9.10	58.51	45.84	4.82	7.53	0.34
+0.208	7.40	67.14	51.12	5.15	7.87	0.31
+0.106	4.40	80.04	51.65	7.07	7.36	0.29
+0.074	10.00	83.82	53.84	4.49	6.35	0.25
−0.074	22.60	100.00	46.18	5.37	5.91	0.11
Total	100.0		47.52		7.16	
Original	100.0		51.94	11.67	8.73	0.199

Table 4. Minerals constitution of major and minor components of the −6.0 + 2.10 mm fraction.

Mineral	Major components						Minor components			
	1	2	3	4	5	6	7	8	9	10
Clinochlore	40.0	31.6	2.1	---	40.8	12.5				
Hornblende	23.5	31.6	6.4	---	19.1	37.4				
Quartz	12.6	13.6	33.6	35.4	10.4	21.3	38.0	74.2		
Talc	13.1	13.8	---	---	19.5	---				
Albite	6.1	11.0	35.6	38.7	---	14.3				
Biotite	4.0	5.9	4.9	4.7	5.9	6.8				
Microcline	---	---	17.4	21.2	---	---				
Cassiterite	0.15	0.18	0.26	0.31	0.12	7.70	8.5			
Topaz							53.4	25.8		

Table 5. Size/chemical analysis of the ground sample.

Fraction, mm	Wt%	SiO_2%	Al_2O_3%	SnO_2%	Dist., %
−0.5 + 0.211	50.75	52.91	14.09	0.179	35.71
−0.211 + 0.074	11.56	55.52	6.91	0.239	10.85
Total	62.31			0.190	59.49
−0.074	37.59	51.62	8.77	0.21	40.51
Calculated	100.00			0.199	100
Original sample	100.00	51.94	11.87	0.199	100

Results of sink/float tests using bromoform (sp.g. 2.89 g/cc) showed that 24.40% and 21.40% by weight of the ground −0.51 + 0.211 mm, and −0.211 + 0.074 mm samples were separated as heavy products with increase in MgO from 10.97% to 13.38%, TiO_2 from 0.75% to 1.02%, Cr_2O_3 from 0.17% to 0.47%, and Fe_2O_3 from 8.73% to 14.38% (Table 6). On the other hand, the silica and alumina contents assayed 46.16% SiO_2, and 10.04% Al_2O_3, respectively (Table 6). The increase in content of these oxides may be attributed to the presence of tremolite, hornblende, and biotite granites in the sink fraction. Meanwhile, SnO_2 content increased from 0.199% in the original sample to 0.76% in the sink product (Table 6). This showed that almost all the cassiterite content in the original sample was concentrated as inclusions of different concentrations within the matrices of these heavy minerals.

Petrography investigation of polished sections of these samples' cuts showed that cassiterite inclusions were found almost throughout all the minerals matrices granitic formations in different concentrations and with various diameter sizes between 120 microns to 5 microns as shown in Figure 4 as follows:

- Thin veins and grains of cassiterite (from 20 to 120 um) found in the fractured quartz (Figure 4(A)).
- Patches of cassiterite (from 30 to 5 um in diameter) coating the surface of biotite (Figure 4(B)).
- Finely disseminating elongate crystals of cassiterite (from 10 to 5 um diameter) found in groundmass of Hornblende and Biotite (Figure 4(C)).

- Large crystal of cassiterite "Hexagonal" (150 um diameter) (**Figure 4(D)**).
- Very large crystal of cassiterite (from 200 - 250 um diameter) (**Figure 4(E)**).
- Large cassiterite particle (120 um diameter) and large vein of cassiterite found between biotite and hornblende (light brown in color) (**Figure 4(F)**).
- Grains of cassiterite (from 40 - 120 um in diameters) found in the open space between quartz and microcline (**Figure 4(G)**).
- Grains of cassiterite (from 40 - 120 um in diameters) found in the open space between quartz and microcline (yellow brown in color) (**Figure 4(H)**) and (**Figure 4(I)**).
- Large grains of elongated cassiterite and topaz minerals were detected together in the 400 microns particle size (**Figure 4(J)**).

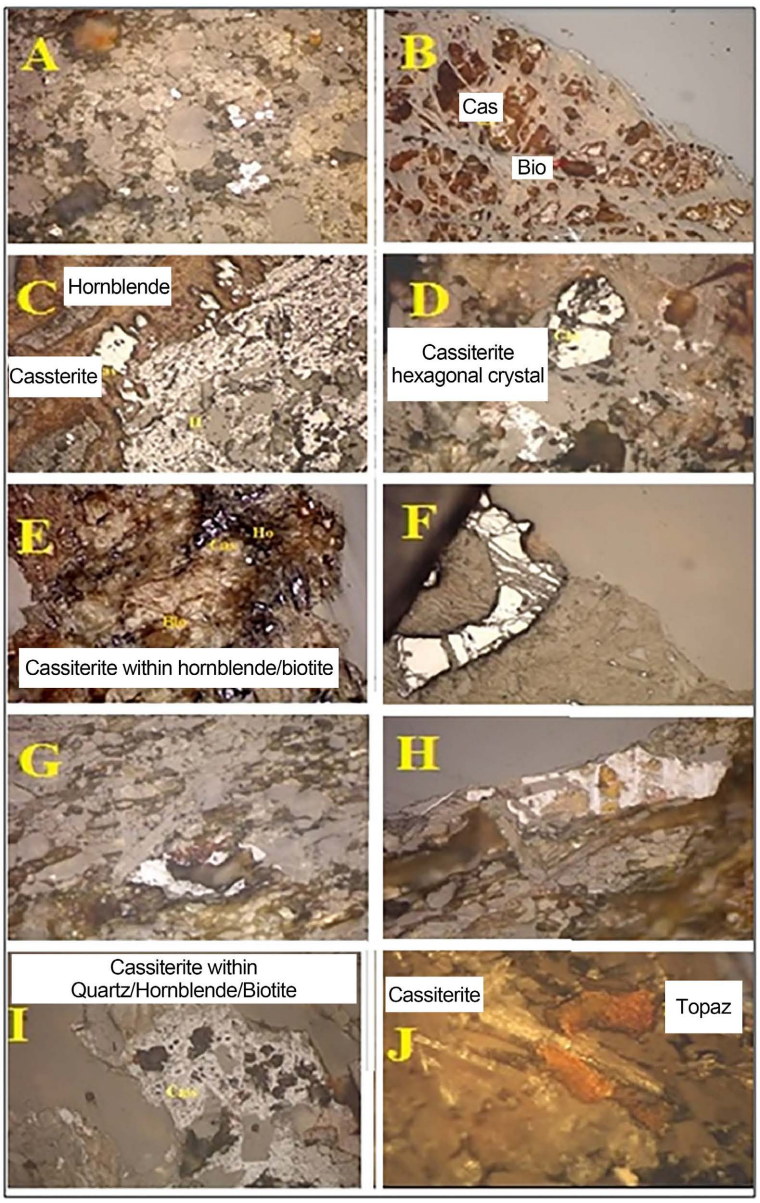

Figure 4. Micro-photos of cassiterite inclusions within various mineral ground-masses.

Table 6. XRF analysis of −0.51 + 0.074 mm ground sample (sink fraction).

Oxide	Wt%	Oxide	Wt%
Na_2O	0.51	CuO	0.004
MgO	13.38	ZnO	0.012
Al_2O_3	10.04	As_2O_3	0.003
SiO_2	46.19	Rb_2O	0.010
P_2O_5	0.17	SrO	0.010
SO_3	0.02	Y_2O_3	0.004
K_2O	0.66	ZrO_2	0.009
CaO	6.76	Nb_2O_5	0/006
TiO_2	1.02	SnO_2	0.759
Cr_2O_3	0.47	PbO	0/012
MnO	0.65	Cl	0.001
Fe_2O_3	14.38	Br	0.012
NiO	0.104		

3.2. Cassiterite Enrichment Using Shaking Table

Several exploratory experiments were conducted to separate the −0.51 + 0.21 mm fraction sample using "Wilfley" shaking table. It was remarked that the feeding rate 1.30 kg/min with 25% solid and wash water flow rate 20 l/min were suitable working conditions to proceed reasonable separation on the table surface. By applying these conditions at table inclination 3˚, there was no notable qualitative improvement on the segregation process (which was easily to follow up due to the pronounced differences in color) at various stroke lengths 2.0, 2.5, 3.0 cm. By increasing the table inclination to 4˚ and 5˚, no remarkable changes were noticed (**Figure 5**). However, at table inclination 5˚ and stroke length 2.5 cm, the wash water flow rate seemed very effective on the separation process. It was noticed that by increasing the water flow rate to 25 l/min, an improving in the separation process was occurred (**Figure 6**). This information proved that the wash water flow rate was a detrimental parameter on the table separation efficiency in this case study. As the wash water flow rate increased, the transport of light minerals to the tailings fraction increased which in turn improved the grade of the heavy concentrate portion. however, a remarkable narrow black strip fraction was observed at the far end of the deck towards the wash water source was produced at table inclination 5˚, stroke length 2.5 cm, and table speed 280 - 300 rpm.

In case of applying the finer fractions −0.21 + 0.074 mm, the suitable stroke length was reduced to 2 cm with increased table speed up to about 320 - 330 rpm. Usually the increase in the length of the stroke required a decrease in the number of strokes per minute and vice-versa to achieve efficient separation. High amplitude was necessary when treating relatively coarse particles in order to create complete dilation along with lower acceleration [23] [35] [36] [37] [43] [44].

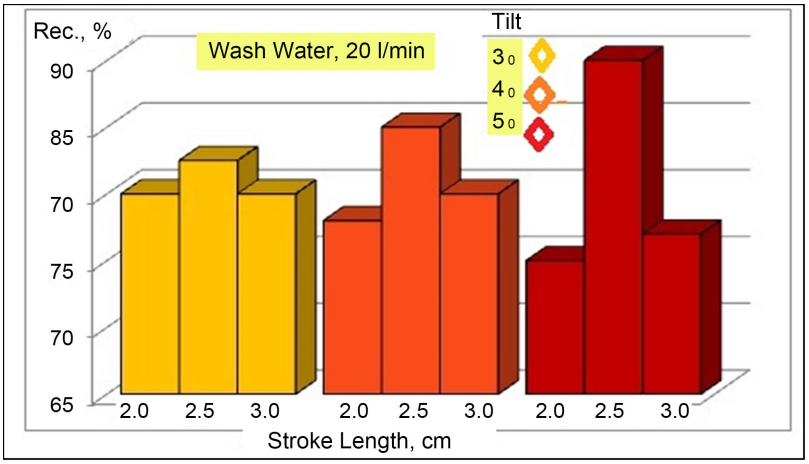

Figure 5. Effect of stroke length at different table inclinations on cassiterite recovery%.

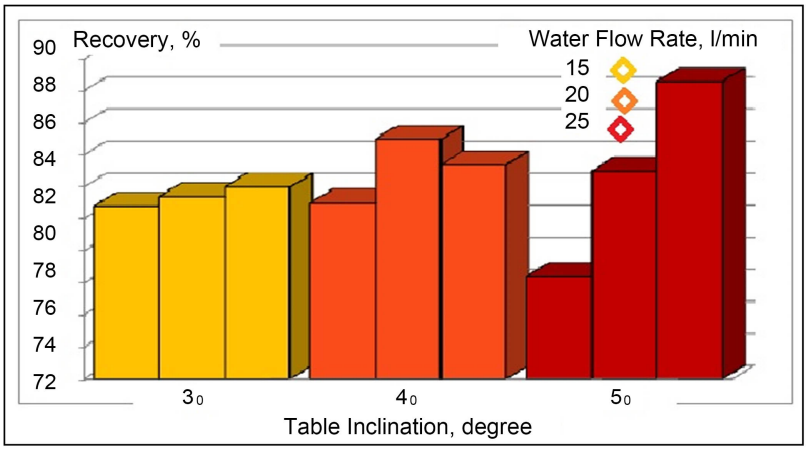

Figure 6. Effect of table inclination at different wash water flow rates on cassiterite recovery%.

At optimum conditions of both fractions, an overall shaking table concentrate was obtained with 0.29% SnO_2 and an operational recovery reached 96.94% from a feeding contained 0.19% SnO_2. The Schematic diagram showing the shaking tabling separation process was shown in **Figure 7**. The evaluation of the final end-products with respect to cassiterite recovery and grade after shaking table was illustrated in **Table 7** and **Figure 8**.

3.3. Statistical Optimization of RER Separation of Cassiterite Concentrates

The statistical design summary and results of the rare earth roll (RER) separator process in terms of cassiterite recovery% as a response are shown in **Table 8** and **Table 9**. It can be seen that the cassiterite recovery% reached an optimum level of 97% (runs 2, 5, 7, 8, 10, and 11) at splitter angle 72.50˚, and at belt speed 150.00 rpm. A regression equation was obtained by multiple regression analysis of the experimental data shown as follows:

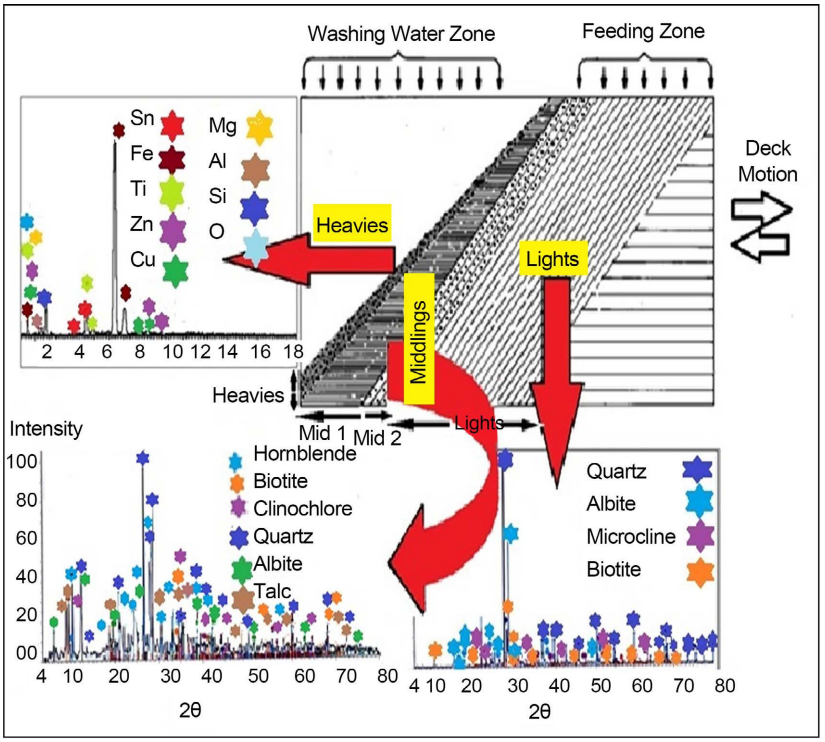

Figure 7. Schematic diagram illustrating shaking table separation process.

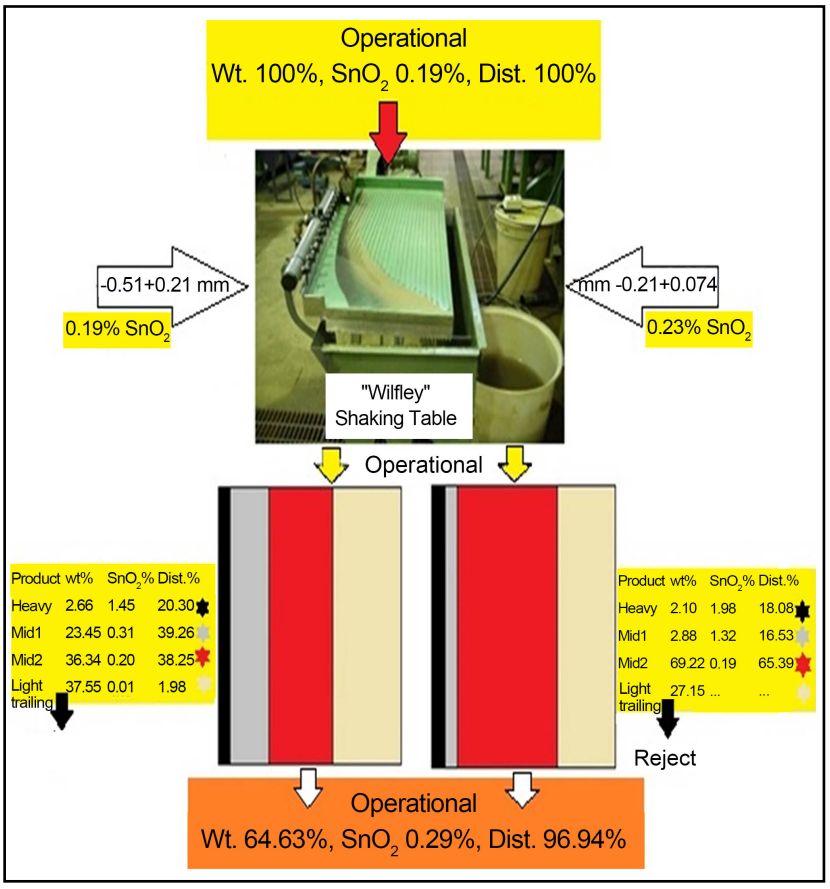

Figure 8. Schematic diagram showing the shaking tabling processing flow-sheet.

Table 7. Evaluation of shaking table products.

Product	−0.51 + 0.211 mm			−0.211 + 0.074 mm			−0.51 + 0.074 mm		
	Wt%	SnO_2%	SnO_2% Dist.$_{opt.}$	Wt%	SnO_2%	SnO_2% Dist.$_{opt.}$	Wt%	SnO_2%	Dist., %
Heavy	2.66	1.45	20.30	2.10	1.98	18.08			
Middling 1	23.45	0.31	39.26	2.88	1.32	16.53			
Middling 2	36.34	0.20	38.25	69.22	0.19	65.39			
Light tailing	37.55	0.01	1.98	27.15	---	---			
Calc. opt.	100.00	0.190	100.00	100.0	0.23	100			
Feed (overall)	50.75	0.190	47.75	11.56	0.23	11.45	62.31	0.19	60.49
Conc. (overall)							40.27	0.29	58.64

Table 8. Design summary.

Stydy type				Response surface			
Experiments				13			
Initial design				Central composite			
Blocks				No blocks			
Design model				Quadratic			
Responce	Name	Units	Obs	Minimum	Maximum	trans	Model
Y1	recovery	%	13	86.00	97.00	None	Quadratic
Factor	Name	Units	Type	Low actual	High actual	Low coded	High coded
A	Splitter angle	Degree	Numeric	70.00	75.00	−1.000	1.000
B	Belt speed	rpm	Numeric	100.00	200.00	−1.000	1.000

Table 9. Results of the full factorial design.

Std	Run	Block	Variable 1 A: Splitter angle, degree	Variable 2 B: belt speed, rpm	Response 1 Recovery %
3	1	Block 1	70.00	200.00	90.00
8	2	Block 1	72.50	220.71	97.00
2	3	Block 1	75.00	100.00	96.00
1	4	Block 1	70.00	100.00	86.00
9	5	Block 1	72.50	150.00	97.00
4	6	Block 1	75.00	200.00	96.00
12	7	Block 1	72.50	150.00	97.00
10	8	Block 1	72.50	150.00	97.00
6	9	Block 1	76.04	150.00	96.00
11	10	Block 1	72.50	150.00	97.00
13	11	Block 1	72.50	150.00	97.00
7	12	Block 1	72.50	79.29	86.00
5	13	Block 1	68.96	150.00	90.00

$$\text{Recovery\%} = -24.76 + 66.22 * A + 0.68 * B - 0.44 * A^2 - 3.00E - 004 * B^2 - 8.00E - 003 * A * B$$

where, A is the splitter inclination angle, and B is the separator belt speed. The optimization of the equation was performed using State-Ease program, by an iteration method. Statistical testing of the model has been carried out by F-test to produce ANOVA—the analysis of variance (Table 10). The values of R^2 and the standard deviation suggested that was in a good agreement between the experimental and predicted values obtained from the model (Figure 9). On the other hand, the effect of both variables and their interaction effect on the mineral recovery were shown in Figure 10 and Figure 11 respectively. Response surface for cassiterite recovery% as function of the separator variables splitter angle, and belt speed was illustrated in Figure 12.

Results showed that with increasing both splitter angle and belt speed to 72.50˚ and 150 rpm, cassiterite recovery increased to reach its maximum at 97% (Figure 13). It was noticed that at low belt speed of 100 rpm, the increase in splitter angle was accompanied by gradual increase in cassiterite recovery from 86% to 92%, and then to 96%. However, at belt speed of 150 rpm, the change in splitter angle showed promising recovery reaching 90% at 70˚, and then the recovery increased to reach 97% at splitter angles 75˚. Additionally, the same trend was shown by increasing the belt speed to reach 200 rpm (Figure 13).

The effect of the feeding material particle size on the efficiency of the rare earth roll separation showed that when nonmagnetic particles travel over a roll and allowed to drop unhindered, they were classified by their particle size, i.e. large particles travelled further from the centerline of the roll than smaller particles. Therefore, large particles are typically processed using lower surface speeds

Table 10. ANOVA response surface quadratic model in terms of recovery% as a responce.

Source	Sum of squares	DF	Mean square	F Value	Prob > F
Model	134.63	5	26.93	6.97	0.0121
A	*74.94*	I	74.94	19.39	0.0031
B	*2.00*	I	2.00	0.52	0.4593
A^2	*52.61*	I	52.61	13.61	0.0078
B^2	*3.91*	I	3.91	1.01	0.3479
AB	*4.00*	I	4.00	1.03	0.3429
Residual	27.06	7	3.87		
Lack of Fit	*27.06*	3	9.02		
Pure Erro	0.000	*4*	*0.000*		
Cor Total	*161.69*	*12*			

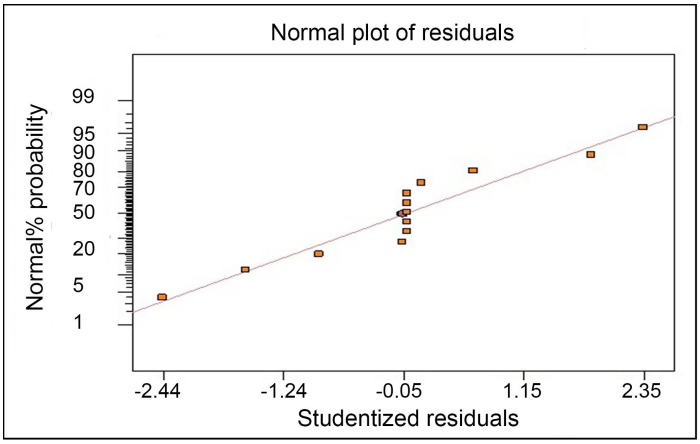

Figure 9. Normal plot of residuals.

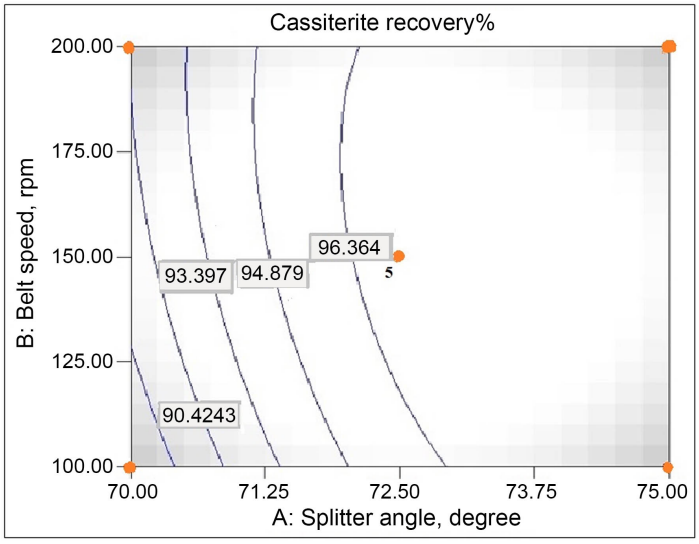

Figure 10. Effect of variables on cassiterite recovery%.

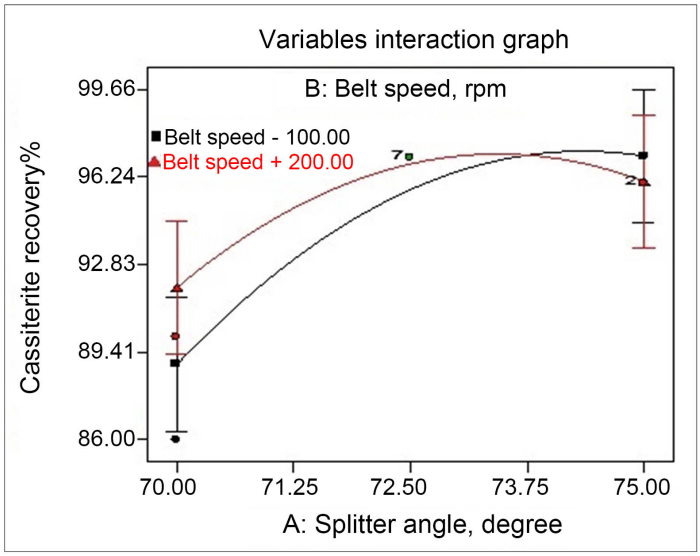

Figure 11. Variables interaction effect on cassiterite recovery%.

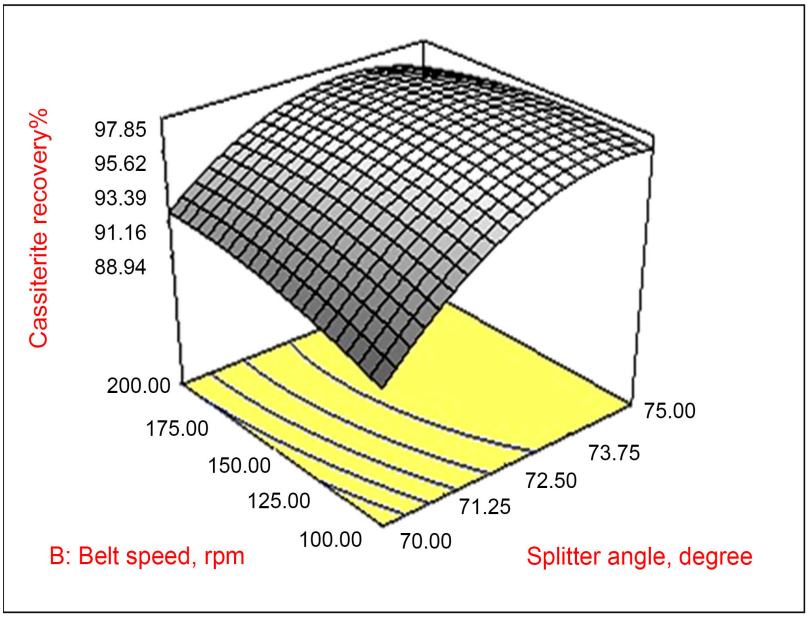

Figure 12. Response surface for cassiterite recovery% as function of "RER" variables.

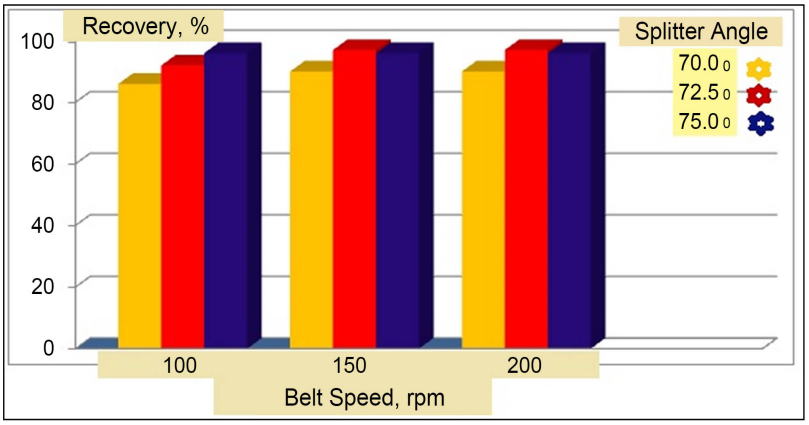

Figure 13. Effect of belt speed at different splitter angles on cassiterite recovery%.

than small particles. When a magnetic roll is used, strongly attached magnetic particles are being usually pinned to the roll surface until they are released from the magnetic field. Weakly attached magnetic particles may only be deflected by the magnetic field, altering them from their normal path. When this occurs, there will be an overlap in the large weakly attached magnetic particles and the small nonmagnetic particles. If the splitter is set to eliminate the large weakly attached magnetic particles, many of the small nonmagnetic particles will report to the magnetic product. On the other hand, if the splitter is set to recover the small nonmagnetic particles, the nonmagnetic product will contain many of the large weakly attached magnetic particles. This is an indication that the particle size range of the feeding material is too great. The problem can normally be overcome by screening the feed before magnetic separation and thus produce a bet-

ter product. The practicality of screening is ultimately based on the difference in the magnetic responses of the particles to be separated and the value of the product(s). That was the way that the present study started by a fractionated feeds −0.51 + 0.21 mm and −0.21 + 0.074 mm.

However, it could be concluded that the optimum separation conditions were reached by keeping the splitter angle fixed at 72.50˚ for both fractions and at belt speeds 150 rpm for coarse fraction and 200 rpm for finer fraction. At these conditions, a coarse concentrate product with 2.10 wt%, 12.96% SnO_2, and 97.62% operational recovery from a feed containing 0.29% SnO_2 was produced. On the other hand, a finer concentrate product with 3.72 wt%, 6.21% SnO_2, and 90.00% operational recovery from a feed containing 0.28% SnO_2 was produced (Table 11). From these results, it could be stated that an overall final cassiterite concentrate with 2.29 wt%, 11.25% SnO_2, and 94.08% operational recovery from a feed contained 0.19% SnO_2, was produced. Important to mention that a non-magnetic product containing topaz mineral was separated from the coarse fraction −0.51 + 0.21 mm only at splitter angle of 65˚ and belt speed 150 rpm. This may be attributed to the presence of topaz that was impeded as inclusions within the hard quartzite matrix, resisted over-grinding and remained in the coarser size 0.50 + 0.21 mm. Block diagram illustrating the magnetic separation products was illustrated in Figure 14, putting into consideration that the drawn values of SnO_2% was multiplied by 50 to facilitate the illustration. A schematic diagram showing phase analyses of different separation products was shown in Figure 15. SEM/EDX analyses of topaz mineral, cassiterite/topaz, and cassiterite mineral were illustrated in Figures 16-18. However, the schematic diagram for the suggested processing flow-sheet to recover cassiterite and topaz minerals from the studied scrap sample was illustrated in "Figure 19".

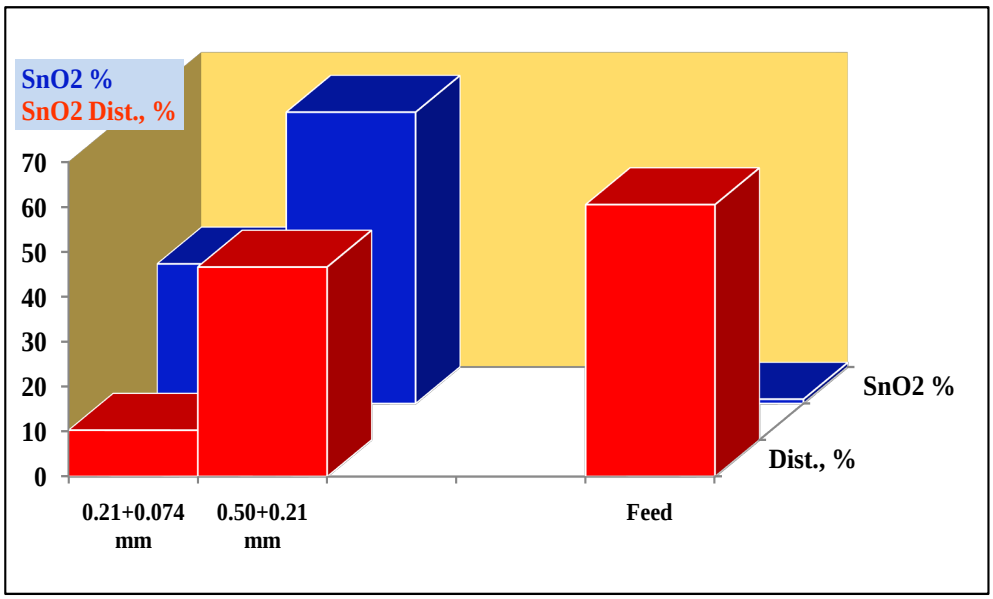

Figure 14. Block diagram showing the evaluation of the magnetic separation process.

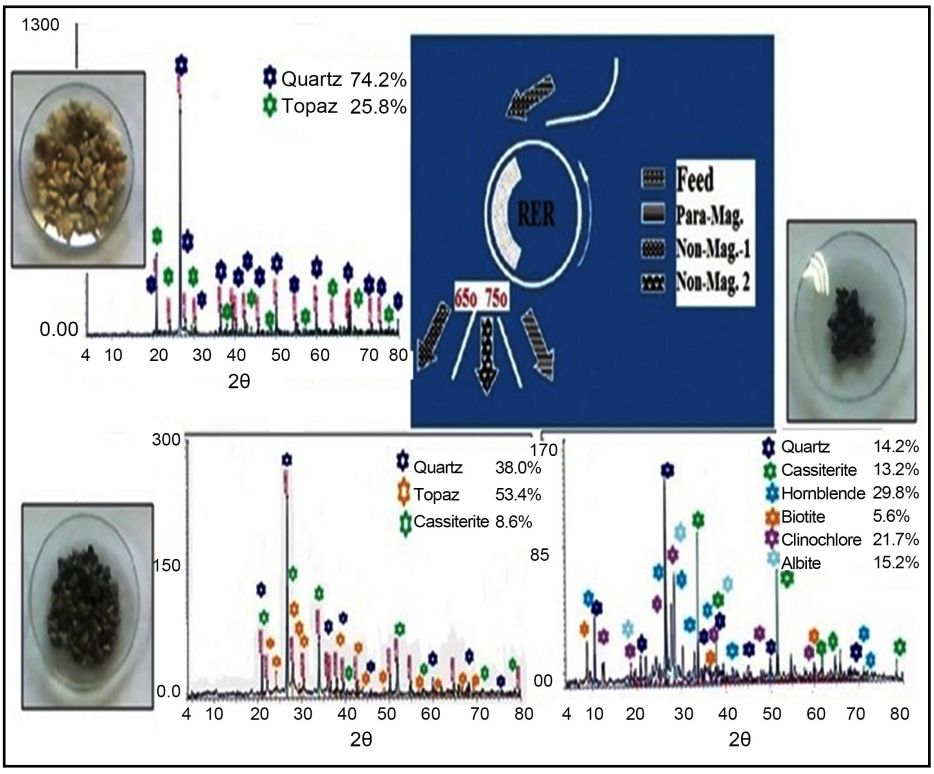

Figure 15. Schematic diagram showing the phase analysis of the magnetic separation process.

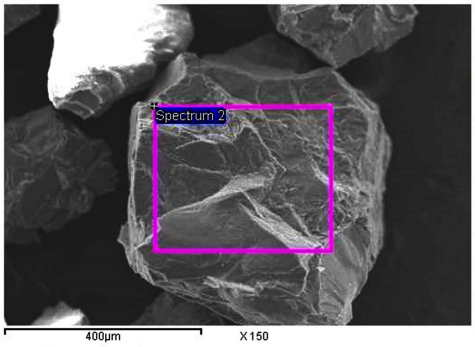

Element	App Conc.	Intensity Corm.	Weight%	Weight% Sigma	Atomic%
O K	243.20	0.8329	38.04	0.61	48.77
F K	23.67	0.1796	17.18	0.88	18.54
Mg K	1.47	0.5784	0.33	0.09	0.28
Al K	137.17	0.7089	25.21	0.38	19.16
Si K	67.80	0.5209	16.96	0.30	12.38
K K	4.45	0.9121	0.63	0.06	0.33
Fe K	1.66	0.8533	0.25	0.07	0.09
Cu K	5.07	0.8250	0.80	0.12	0.26
Zn K	3.74	0.8247	0.59	0.14	0.19
Totals			100.00		

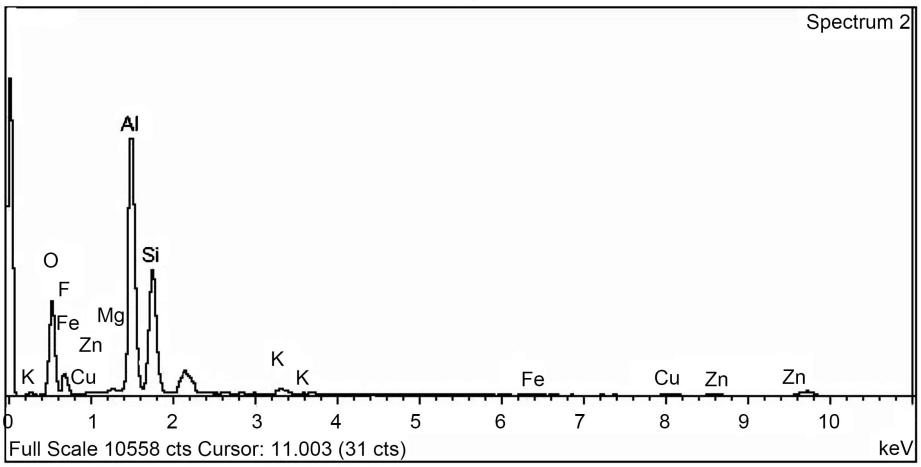

Figure 16. SEM/EDX analyses of separated topaz concentrate.

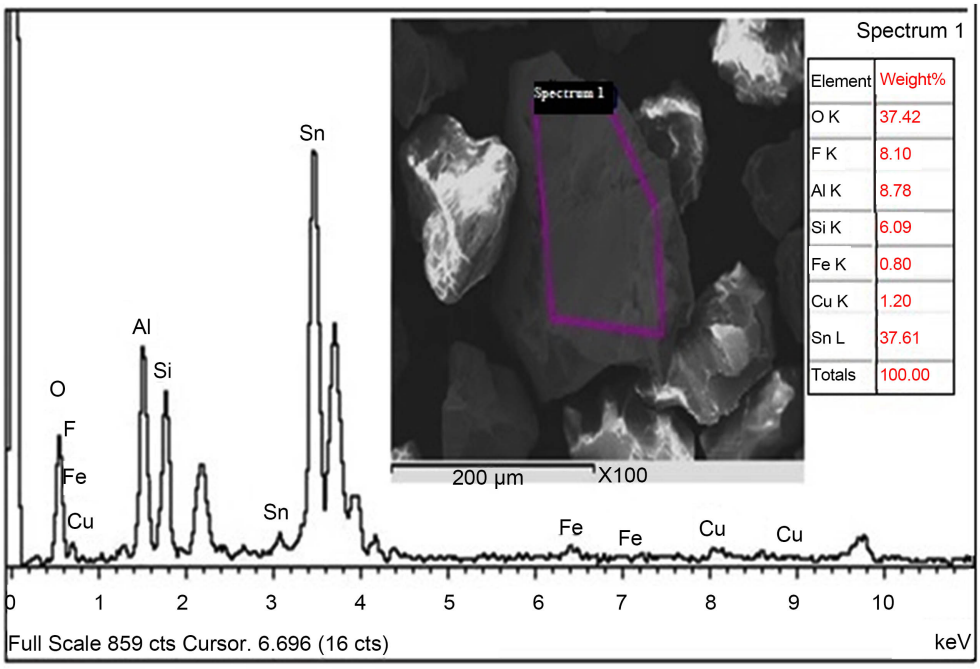

Figure 17. SEM/EDX analyses of cassiterite/topaz concentrate.

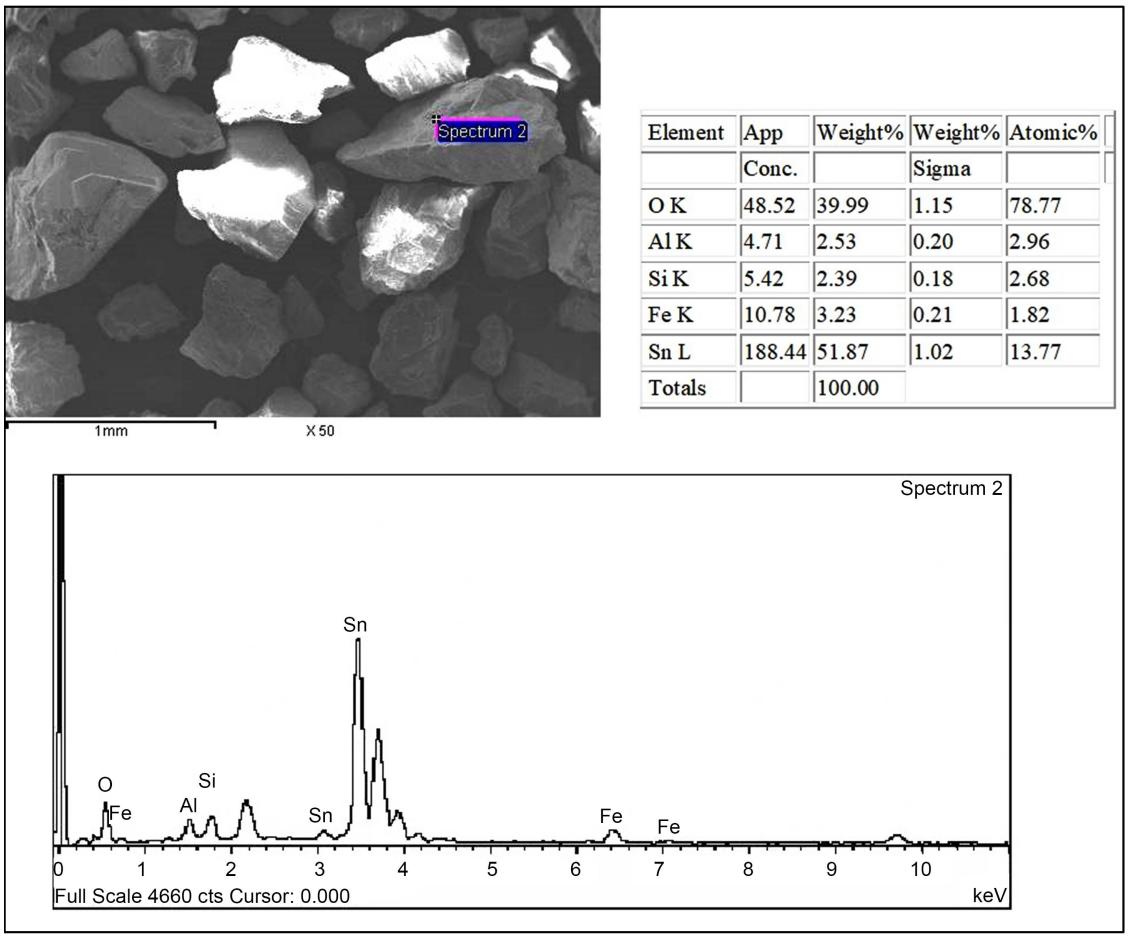

Figure 18. SEM/EDX analyses of cassiterite concentrate.

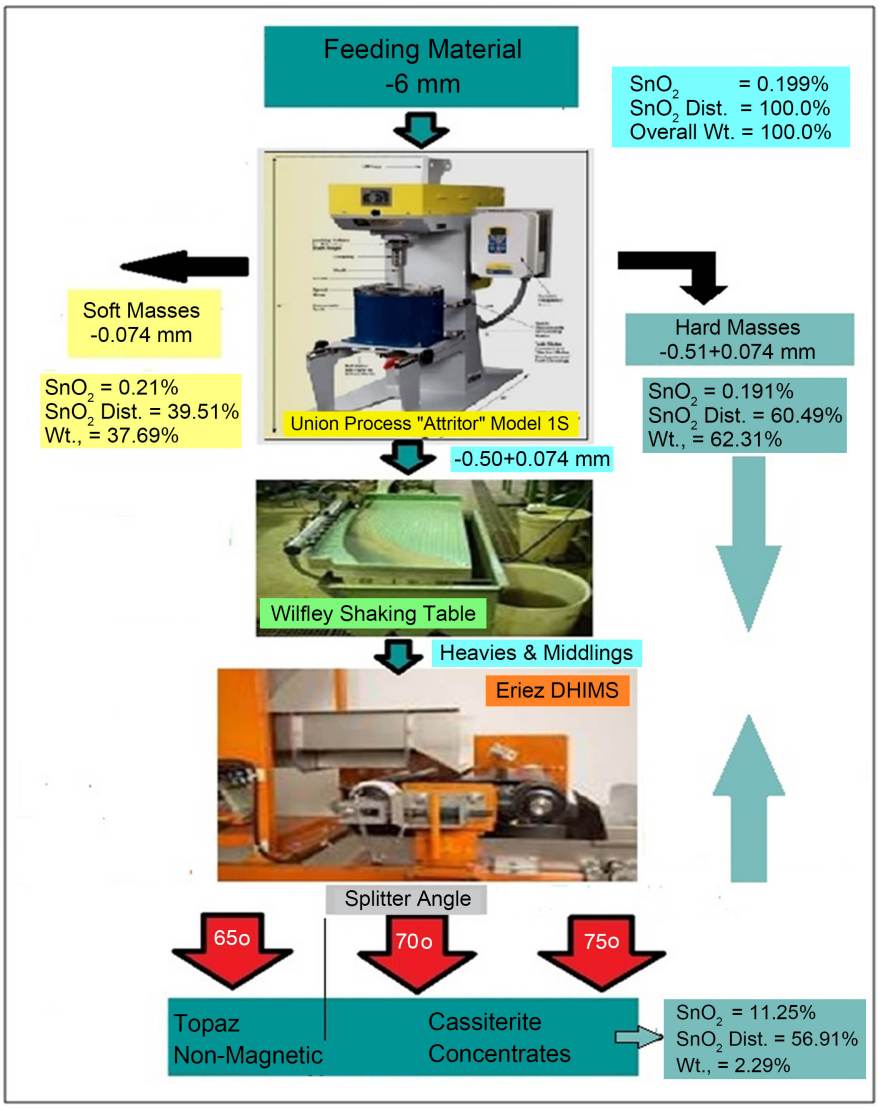

Figure 19. Schematic diagram illustrating the suggested processing flow-sheet.

Table 11. Dry high intensity magnetic separation results.

Angle		−0.51 + 0.21 mm			−0.21 + 0.074 mm		
	Product	Wt%	SnO_2%	Dist., % (opt.)	Wt%	SnO_2%	Dist., % (opt.)
65˚	topaz	7.60	0.01	0.43			
70˚ - 75˚	conc. (opt.)	2.10	12.96	95.48	3.72	6.21	82.55
	feed (Opt.)	62.45	0.29	97.81	74.20	0.28	91.74
	feed total	50.75	0.190	47.75	11.56	0.23	11.45
70˚ - 75˚	total conc.	1.71	12.96	46.61	0.58	6.21	10.30
70˚ - 75˚	overall conc.	2.29	11.25	56.91			
overall feed		62.31	0.19	60.49			
final cassiterite conc.		2.29	11.25	94.08			

4. Conclusions

A technological sample from the mine's scraps of the Eastern Desert of Egypt was subjected to chemical and mineralogical investigation. The sample was below 6 mm in size. It was shown to contain 0.199% cassiterite mineral (SnO_2). Cassiterite mineral was found in different sizes particulates from 250 microns to 5 microns imbedded in granitic ground mass containing quartz—feldspar-hornblende-clinochlore-tremolite-biotite—and talc minerals of different contents in the rock.

Stirring ball milling was adapted to mill the sample into 100% −0.51 mm with minimum fines below 0.074 mm (reached 37.69 wt.%, with 39.51% cassiterite distribution. This fine product was kept aside for a separate study.

The attrition −0.51 + 0.074 mm product was shown to contain about 0.19% SnO_2 with cassiterite distribution reached about 60.49% of the original sample. This product was divided into two fractions, −0.51 + 0.21 mm and −0.211 + 0.074 mm, and subjected separately to "Wilfley" shaking table.

At optimum separation conditions: table surface inclination 5˚, stroke length 2.5 cm, and table speed 280 - 300 rpm for the coarse fraction, and at 2 cm, 4˚, and 320 - 330 rpm for the finer size fraction, an overall concentrate assayed 0.29% SnO_2 with a recovery reaching 96.94% from a feeding material containing 0.19% SnO_2, was obtained.

The heavies and the two middling products after shaking table were directed after dryness to "Eriez" Rare Earth Roll separator, where the light products were rejected. At magnetic field strength approaching 21,000 gauss and feeding rate 2 kg/hr., mathematically designed experiments were applied to optimize the separation process.

At optimum conditions 72.50˚ splitter angle and belt speed 150 rpm, 200 rpm for the two size fractions, respectively, a cassiterite concentrate of 2.29% overall weight, 11.25% SnO_2 with an operational recovery 94.08%, was obtained. In addition, a high-grade topaz mineral product was separated from the coarse fraction −0.50 + 0.211 mm, as a non-magnetic fraction at splitter angle 65˚.

Declarations

- No funds, grants, or other support was received.
- The authors have no conflicts of interest to declare that are relevant to the content of this article.
- All authors certify that they have no affiliations with or involvement in any organization or entity with any financial interest or non-financial interest in the subject matter or materials discussed in this manuscript.
- The authors have no financial or proprietary interests in any material discussed in this article.

Conflicts of Interest

The authors declare no conflicts of interest regarding the publication of this paper.

References

[1] El Aref, M., Abd El-Rahman, Y., *et al.* (2020) Mineral Resources in Egypt (I): Metallic Ores. In: Hamimi, Z., *et al.*, Eds., *The Geology of Egypt. Regional Geology Reviews*, Springer, Cham, 521-587. https://doi.org/10.1007/978-3-030-15265-9_14

[2] Yang, J.G., Wu, Y.T. and Zhang, X.L. (2014) Study on Separation of Tin from a Low-Grade Tin Concentrate through Leaching and Low-Temperature Smelting Processes. *Mineral Processing and Extractive Metallurgy*, **123**, 228-233. https://doi.org/10.1179/1743285514Y.0000000070

[3] Angadi, S.I., Sreenivas, T., Jeon, H.S., Baek, S.H. and Mishra, B.K. (2015) A Review of Cassiterite Beneficiation Fundamentals and Plant Practices. *Minerals Engineering*, **70**, 178-200. https://doi.org/10.1016/j.mineng.2014.09.009

[4] Kumar, N., Joshi, B. and Asokan, K. (2019) The Effects of Thermal Annealing on the Structural and Electrical Properties of Zinc Tin Oxide Thin Films for Transparent Conducting Electrode Applications. *Physica B: Condensed Matter*, **558**, 5-9. https://doi.org/10.1016/j.physb.2019.01.016

[5] Nandi, A., Mandal, S., *et al.* (2019) Application of Hybrid rGO-ITO Bilayer TCO on a-Si Solar Cell for Performance Enhancement. *IEEE Journal of Photovoltaics*, **9**, 12-17. https://doi.org/10.1109/JPHOTOV.2018.2873707

[6] Dalimunthe, D.Y., Aldila, H. and Nuryadin, A. (2020) Optimization on the Purification of Cassiterite from Low-Grade Cassiterite Concentrate. *IOP Conference Series: Earth and Environmental Science*, **599**, Article ID: 012002. https://doi.org/10.1088/1755-1315/599/1/012002

[7] Yang, J.L., Shuai, Z.C., Zhou, W.T. and Ma, S.J. (2019) Grinding Optimization of Cassiterite-Polymetallic Sulfide Ore. *Minerals*, **9**, Article No. 134. https://doi.org/10.3390/min9020134

[8] Falcon, L.M. (1982) The Gravity Recovery of Cassiterite. *Journal of the South Africa Institute of Mining and Metallurgy*, **4**, 112-117.

[9] Sreenivas, T. and Padmanabhan, N.P.H. (2002) Surface Chemistry and Flotation of Cassiterite with Alkyl Hydroxamates. *Colloids and Surfaces A: Physicochemical and Engineering Aspects*, **205**, 47-59. https://doi.org/10.1016/S0927-7757(01)01146-3

[10] Pecina, E.T., Rodriguez, M., Castillo, P., Diaz, V. and Orrantia, E. (2009) Effect of *Leptospirillum ferrooxidans* on the Flotation Kinetics of Sulphide Ores. *Minerals Engineering*, **22**, 462-468. https://doi.org/10.1016/j.mineng.2008.12.008

[11] Bulatovic, S.M. (2020) Handbook of Flotation Reagents: Chemistry, Theory and Practice, Flotation of Sulfide Ores. Elsevier Ltd., Amsterdam.

[12] Gonzales, L.G.V., Pino, G.A.H. and Torem, M.L. (2013) Eletro-Flotation of Cassiterite Fines Using a Hydrophobic Bacterium Strain. *Rem: Revista Escola de Minas*, **66**, 507-512. https://doi.org/10.1590/S0370-44672013000400016

[13] Baba, A.A., Yusuf, A.O., Ragi, M.A., *et al.* (2020) Potential of a Nigerian Cassiterite Ore for Industrial Steel Coatings. In: Azimi, G., *et al.*, Eds., *Rare Metal Technology*, Springer, Cham, 201-208. https://doi.org/10.1007/978-3-030-36758-9

[14] Zhou, Y.C., Tong, X., Song, S.X. and Wang, W. (2014) Beneficiation of Cassiterite Fines from a Tin Tailing Slime by Froth Flotation. *Separation Science and Technology*, **49**, 458-463. https://doi.org/10.1080/01496395.2013.818036

[15] Tian, M.J., Gao, Z.Y., Han, H.S., Sun, W. and Hu, Y.H. (2017a) Improved Flotation Separation of Cassiterite from Calcite Using a Mixture of Lead (II) Ion/Benzohydroxamic Acid as Collector and Carboxymethyl Cellulose as Depressant. *Minerals Engineering*, **113**, 68-70. https://doi.org/10.1016/j.mineng.2017.08.010

[16] Tian, M.J., Hu, Y., Sun, W. and Liu, R. (2017b) Study on the Mechanism and Application of a Novel Collector Complexes in Cassiterite Flotation. *Colloids and Surfaces A*: *Physicochemical and Engineering Aspect*, **522**, 635-641. https://doi.org/10.1016/j.colsurfa.2017.02.051

[17] Tian, M.J., Gao, Z.Y., et al. (2018) Selective Flotation of Cassiterite from Calcite with Salicylhydroxamic Acid Collector and Carboxymethyl Cellulose Depressant. *Minerals*, **8**, Article No. 316. https://doi.org/10.3390/min8080316

[18] Tian, M.J., Zhang, C., Han, H.S., Liu, R., Gao, Z.Y., Chen, P. and He, J. (2018) Novel Insights into Adsorption Mechanism of Benzohydroxamic Acid on Lead (II)-Activated Cassiterite Surface: An Integrated Experimental and Computational Study. *Minerals Engineering*, **122**, 327-338. https://doi.org/10.1016/j.mineng.2018.04.012

[19] Tian, M.J., Liu, R., *et al.* (2018) Activation Mechanism of Fe (III) Ions in Cassiterite Flotation with Benzohydroxamic Acid Collector. *Minerals Engineering*, **119**, 31-37. https://doi.org/10.1016/j.mineng.2018.01.011

[20] Tian, M.J., Gao, Z.Y., Sun, W., Han, H.S., Sun, L. and Hu, Y.H. (2018) Activation Role of Lead Ions in Benzohydroxamic Acid Flotation of Oxide Minerals: New Perspective and New Practice. *Journal of Colloid and Interface Science*, **529**, 150-160. https://doi.org/10.1016/j.jcis.2018.05.113

[21] Tian, M.J., Zhang, C., Han, H., Runqing, L., et al. (2018) Effects of the Preassembly of Benzohydroxamic Acid with Fe (III) Ions on its Adsorption on Cassiterite Surface. *Minerals Engineering*, **127**, 32-41. https://doi.org/10.1016/j.mineng.2018.07.019

[22] Tian, M.J., Khoso, S.A., Wang, L., Sun, W., Zhang, C. and Hu, Y. (2019) Selective Separation Behavior and its Molecular Mechanism of Cassiterite from Quartz using Cupferron as a Novel Flotation Collector with a Lower Dosage of Pb^{2+} Ions. *Applied Surface Science*, **486**, 228-238. https://doi.org/10.1016/j.apsusc.2019.05.039

[23] Zhang, L., Khoso, S.A., Tian, M. and Sun, W. (2021) Cassiterite Recovery from a Sulfide Ore Flotation Tailing by Combined Gravity and Flotation Separations. *Physicochemical Problems of Minerals Processing*, **57**, 206-215. https://doi.org/10.37190/ppmp/131006

[24] Wills, B.A. and Napier-Munn, T.J. (2006) Mineral Processing Technology: An Introduction to the Practical Aspects of Ore Treatment and Mineral Recovery. 7th Edition, Butterworth-Heinemann, Oxford. https://doi.org/10.1016/B978-075064450-1/50000-X

[25] Lungu, M. (2009) Separation of Small Nonferrous Particles Using a Two Successive Steps Eddy-Current Separator with Permanent Magnets. *International Journal of Mineral Processing*, **93**, 172-178. https://doi.org/10.1016/j.minpro.2009.07.012

[26] Jiao, H., Shib, C. and Tian, R. (2011) Research on Design and Magnet Assembly Process of Multivariate and Multi-Roll Permanent Magnetic Separator. *Advanced Materials Research*, **201-203**, 486-490. https://doi.org/10.4028/www.scientific.net/AMR.201-203.486

[27] Li, Y.F. and Yang, F.T. (2016) Research Progress and Development Trend of Permanent Magnetic Separators in China and Abroad. 3*rd International Conference on Vehicle*, *Mechanical and Electrical Engineering* (*ICVMEE* 2016), December 9-11 2016, Hong Kong, China. https://doi.org/10.12783/dtetr/icvme2016/4873

[28] Zeng, S., Zeng, W., Ren, L. and Li, H. (2015) Development of A High Gradient Permanent Magnetic Separator (HGPMS). *Minerals Engineering*, **71**, 21-26. https://doi.org/10.1016/j.mineng.2014.10.009

[29] Zong, Q.X., Fu, L.Z. and Bo, L. (2018) Variables and Applications on Dry Magnetic

Separator. 3*rd International Conference on Advances in Energy and Environmental Research*, Guilin, 10-12 August 2018, 1-9.

[30] Slusarek, B. and Zakrzewski, K. (2012) Magnetic Properties of Permanent Magnets for Magnetic Sensors Working in Wide Range of Temperature. *Electrical Review*, **88**, 123-126.

[31] Hisayoshi, K., Uyeda, C. and Terada, K. (2016) Magnetic Separation of General Solid Particles Realized by a Permanent Magnet. *Scientific Reports*, **6**, Article No. 38431. https://doi.org/10.1038/srep38431

[32] Dimova, T., Aprahamian, B. and Marinova, M. (2019) Research of the Magnetic Field Inside a Drum Separator with Permanent Magnets. 2019 16*th Conference on Electrical Machines*, *Drives and Power Systems* (*ELMA*), Varna, 6-8 June 2019, 1-4. https://doi.org/10.1109/elma.2019.8771679

[33] Shvedchykova, I., Melkonova, I. and Romanchenko, J. (2020) Research of Magnetic Distribution in the Working Area of Disk Separator, Taking into Account an Influence of Materials of Permanent Magnets. *EUREKA*: *Physics and Engineering*, No. 1, 87-95. https://doi.org/10.21303/2461-4262.2020.001106

[34] Hu, B., Nakahiro, Y. and Wakamatsu, D.T. (1993) A Study on the Separation of Fine Cassiterite and Quartz by Liquid-Liquid Extraction. *XVIII International Mineral Processing Congress*, Sydney, 23-28 May 1993.

[35] Egbe, E.A.P., Mudiare, E., Abubakre, O.K. and Ogunbajo, M.I. (2013) Effectiveness of Gravity Separation Methods for the Beneficiation of Baban Tsauni (Nigeria) Lead Gold Ore. *International Journal of Scientific and Research Publications*, **3**, 1-4.

[36] Ajaka, E.O., Akande, J.M. and Saliu, M.A. (2014) Design of Comminution Circuit for Optimum Performance of the Gravity Separation Unit at in-take Iron Ore Processing Plant, Nigeria. *Innovative Systems Design and Engineering*, **5**, 28-30.

[37] Mouedhen, I., Coudert, L., Blais, J.F. and Mercier, G. (2018) Study of Factors Involved in the Gravimetric Separation Process to Treat Soil Contaminated by Municipal Solid Waste. *Journal of Environmental Management*, **209**, 23-36. https://doi.org/10.1016/j.jenvman.2017.12.020

[38] Saisinchai, S., Boonpramote, T., Meechumna, P. (2016) Recovery of Fine Cassiterite from Tailing Dump in Jarin Tin Mine, Thailand. *Engineering Journal*, **20**, 41-49.

[39] Su, Z.J., Zhang, Y.B., Liu, B.B., Lu, M.M., Li, G.H. and Jiang, T. (2017) Extraction and Separation of Tin from Tin-Bearing Secondary Resources: A Review. *JOM*, **69**, 2364-2372. https://doi.org/10.1007/s11837-017-2509-1

[40] Go, O., Moc, O and, Gn, O. (2015) Energy Potential of Microwave Heating: Prior to and in Leaching of Low-Grade Kuru Cassiterite Ore in Jos, Nigeria. *FUTO Journal Series* (*FUTOJNLS*), **1**, 78-83.

[41] Lalasari, L.H., Suharyanto, A. and Firdiyono, F. (2017) The Effect of Pretreatments on the Dissolutions of Impurities from Indonesian Cassiterite Mineral. *Journal of Physics*: *Conference Series*, **817**, Article ID: 012064. https://doi.org/10.1088/1742-6596/817/1/012064

[42] EGSMA (1998) Metallogenic Map of Arab Republic of Egypt, Metallic Ores and Non Metallic Deposits, Scale 1:1,000,000. Egyptian Geological Survey and Mining Authority.

[43] Tripathy, S.K., Ramamurthy, Y., Sahu, G.P., Panda, L., Singh, V. and Tathavadkar, V. (2010) Influence of Shaking Table Process Parameters on Concentration of Chromite Plant Tailings. *Proceedings of the XI International Seminar on Mineral Processing Technology* (*MPT*-2010), Jamshedpur, 15-17 December 2010, 199-204.

https://www.semanticscholar.org/paper/Influence-of-shaking-table-process-parameters-on-of-Tripathy-Ramamurthy/dd24019f71c59fa054e5901f969b81d9e8e91786

[44] Burt, B. and Mills, C. (1984) Gravity Concentration Technology. Elsevier, New York.

[45] Box, G.E.P. and Behnken, D.W. (1960) Some New Three Level Designs for the Study of Quantitative Variables. *Technometrics*, **2**, 455-475. https://doi.org/10.1080/00401706.1960.10489912